Impact of Axial Compression for the mMR Simultaneous PET-MR Scanner

Martin A. Belzunce, Jim O'Doherty and Andrew J. Reader

***Abstract*—In 3D PET an axial compression is often applied to reduce the data size and the computation times during image reconstruction. This compression scheme can achieve good results in the centre of the FOV. However, there is a loss in the spatial resolution at off-centre positions and this effect is increased in scanners with a larger FOV. This is the case for the Siemens Biograph mMR, which by default uses an axial compression of span 11. An assessment of the improvement in the spatial resolution that would be achieved in a reconstruction without axial compression, is necessary to evaluate if the additional computational burden is justified for routine image reconstruction. In this work, we present an implementation of the ordinary Poisson ordered subsets expectation maximization (OP-OSEM) algorithm without axial compression for the mMR, and evaluate its performance for span 1 and span 11. We show that an improvement of 3 mm FWHM (i.e. an improvement of 40%) can be achieved when span 11 compression is avoided and the source is at a distance greater than 100 mm from the centre of the FOV. In addition, the general image quality properties of the algorithm were evaluated with a NEMA image quality phantom acquisition and contrasted with its reconstruction via the STIR open source reconstruction software.**

I. Introduction

In 3D PET, an axial compression is used to reduce the data size and the computation times during reconstruction. This is achieved by averaging a set of sinograms with adjacent values of the oblique polar angle [1]. This sampling scheme achieves good results in the centre of the FOV. However, there is a loss in the radial, tangential and axial resolutions at off-centre positions, which is increased in scanners with large FOVs.

The Siemens Biograph mMR was the first simultaneous whole body PET-MR and it has one of the largest FOVs commercially available [2]. The system uses a sinogram-based reconstruction with an axial compression of span 11 and a component-based normalization. Additionally, for each acquisition the scanner stores a span 1 sinogram in interfile format for both the prompt and delayed events. This feature brings the possibility of implementing an image reconstruction algorithm without axial compression that would improve the spatial resolution in the outer regions of the FOV, which could benefit whole body studies.

In this work we present an implementation of a reconstruction algorithm without axial compression for the Biograph mMR. To validate the implementation, we evaluated the image properties of a NEMA Image Quality (IQ) phantom acquisition using a method capable of assessing image quality even if scatter correction is not applied to the data. Finally, we performed an evaluation of the improvement of the spatial resolution when no axial compression is used compared to the standard span 11 reconstruction.

Martin A. Belzunce, Jim O'Doherty and Andrew J. Reader are with King's College London, Division of Imaging Sciences and Biomedical Engineering, St Thomas Hospital, London, UK.

II. Materials and Methods

The standard reconstruction for the scanner Biograph mMR uses span 11 sinograms with 64 rings and a maximum ring difference of 60. Therefore a total of 837 sinograms arranged in 11 segments are stored for each acquisition. Each sinogram has 344 [radial coordinate] $\times$ 252 [azimuthal angle] bins, where no transverse mashing is applied. The system has a transaxial FOV of 59.4 cm and an axial FOV of 25.8 cm. The scanner also permits storage of span 1 sinograms for each acquisition, increasing the number of sinograms to 4084 arranged in 121 segments.

A 3D OP-OSEM reconstruction algorithm [3] was implemented in a C++ library for both span 11 and span 1 sinograms. The projector and backprojector used are based on the Siddon's algorithm [4]. They were implemented in both CPU and GPU versions, where the latter was developed using CUDA [5]. To compute the normalization factors for span 1, and for span 11, the geometric, the crystal interference, the axial profile and the crystal efficiencies factors available in the component-based normalization were used [6]. For the latter, sinograms of span 11 and span 1 were generated from the crystal efficiencies of each crystal element. The axial factors for span 1 were created using a uniform cylinder scan.

The computational cost of each reconstruction is proportional to the number of sinogram bins to process. Thus, the span 1 reconstructions are approximately 5 times more demanding than the span 11 reconstructions. However, the backprojection of zero-bins can be avoided, and, for that reason, the reconstruction of the NEMA phantom took only 3.5 times longer for span 1 than for span 11.

A. NEMA IQ Acquisition

An acquisition with the NEMA IQ phantom was performed to validate the implemented algorithm. The phantom was filled with [^{18}F]FDG only in the background, while the cold spheres were filled with nothing but air. The main goal of this acquisition was to validate the OSEM implementation, including the projector/backprojector, and the computed span 1 normalization factors. For this reason, the sinograms weren't corrected for scatter and randoms events. In order to have a good overall validation of the algorithm, the phantom was reconstructed using 1 subset (ML-EM) and 60 iterations for the span 11 and span 1 sinograms, and with STIR [7], where the span 11 reconstruction for the Biograph mMR has already been validated [8]. For the attenuation correction, we used a CT scan of the phantom registered with an emission image since the attenuation map derived from the MRI scan had some artifacts.

The signal to noise ratio (SNR) was computed for each image as the ratio between the mean value and the standard deviation in the background region of the phantom. Since the images were not corrected for randoms and scatter, a spatially variant bias would

be found in the uniform background and a misleading value of the standard deviation would be obtained. For this reason, we propose a different method to compute the SNR in the images. In this method, we use a spatially variant estimate of the mean value in the background of the phantom. Then we define the standard deviation with spatially-variant mean (SDSVM) as:

$$\sigma_{SVM} = \sqrt{\sum_{j=1}^{J} \frac{(x_j - \mu_j)^2}{J-1}} \quad (1)$$

where x_j is the j pixel of the background region of the phantom, J is the number of pixels that compose the background region and μ_j the mean estimate for the spatial position of pixel j.

In order to get the spatially variant estimate of the mean, we applied a strong low pass filter (a Gaussian kernel of 21×21 pixels with standard deviation of 7 pixels, equivalent to 14.56 mm) to each slice of the reconstructed volume. To avoid edge effects we used a mask for the background region generated from the CT scan of the phantom. At the same time we generated an eroded mask that will be used in the final stage to select the pixels that will be used to compute the standard deviation. A profile of the reconstructed images and of both masks scaled to the mean value of the image can be observed at the top left in Fig. 1. The same filter is applied to the mask (top right in Fig. 1). In the third step, the ratio between the filtered masked image and the filtered mask is computed (bottom left in Fig. 1). Therefore, the edge effect produced by the filter is corrected. Finally, the eroded mask is applied to the resultant image of step 3 and we get an estimate of the mean value in the background region of the phantom using only pixels that are inside the phantom.

Using this spatially variant mean estimate and the standard deviation of Eq. 1 we computed the SNR value of the reconstructed volume for each iteration. Moreover, we obtained the contrast recovery coefficients (CRC) for each of the spheres in the phantom. In this case, we used a similar process to the one described in [9] but using only the two closest background ROIs to each sphere to compute the mean background value.

B. Line Source Acquisition

A line source was used to measure and evaluate the spatial resolution. The line source was located in a oblique direction in the FOV, where the line sweeps from -160 to +180 mm in x, +100 to +105 mm in y and the whole axial length in z (Fig. 3). The volume was reconstructed with OP-OSEM using 21 subsets and 3 iterations, without any post-reconstruction filtering, using our span 1 and span 11 implementations, STIR and the vendor's software. The transverse pixel size was 2.08 mm for all reconstructed images. The full width at half maximum (FWHM) in the x and y axes were computed for each transverse slice and the FWHM in the x and z axes for each sagittal plane. The FWHM was computed using the coordinates of the maximum value for each plane, then analysing each 1D profile centred in the maximum pixel for each axis and obtaining an interpolated coordinate value for the half of the maximum pixel value.

III. Results

The SNR values of the reconstructed images for our code and for STIR were almost equivalent for each iteration. The CRC of

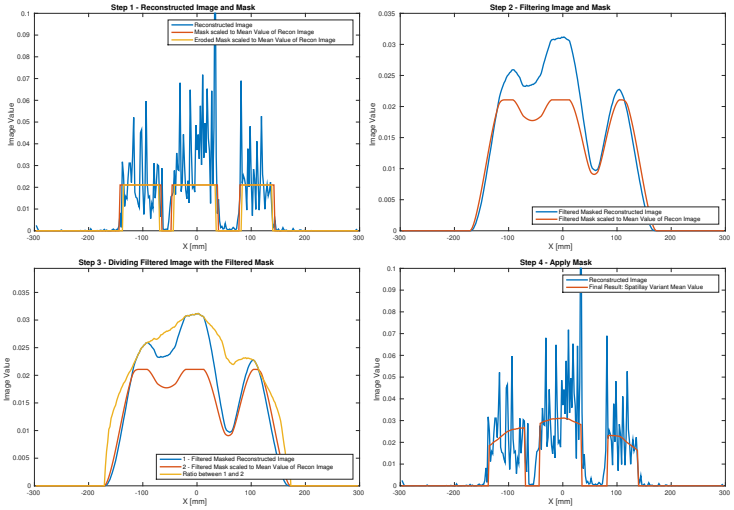

Fig. 1. Profiles of the images used in the process to obtain a spatially variant mean estimate. Top Left: two masks scaled to the mean value of the reconstructed image. Top Right: in step 2 a smoothed image and mask is computed. Bottom Left: in step 3 the ratio between the filtered image and the mask is obtained. Bottom Right: the eroded mask is applied to the ratio of step 3 and it is used as the spatially-variant mean of the image.

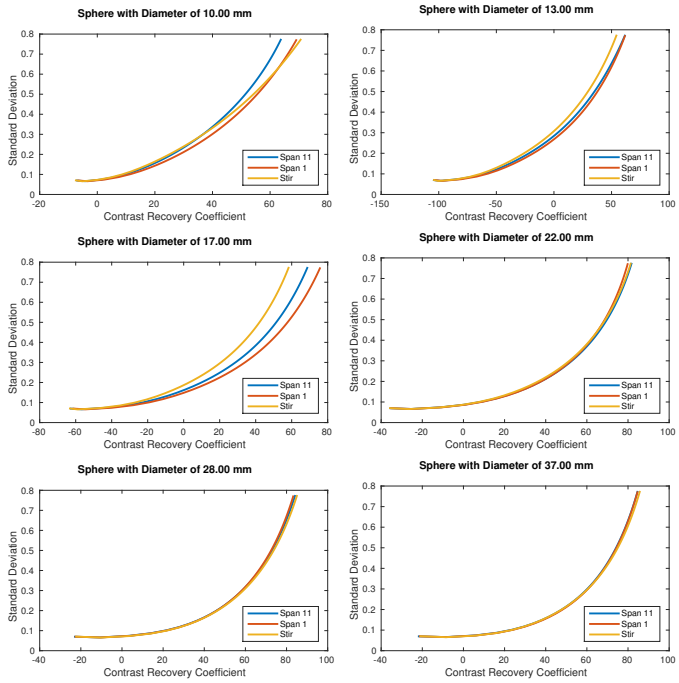

Fig. 2. Plots of the change of Standard Deviation vs CRC with iterations for each sphere in the IQ phantom.

each sphere against the standard deviation of the image is shown in Fig. 2. Similar values were obtained in our implementation as for STIR. The same for the CRC with exception of the 17 mm diameter sphere, where the span 1 code shows a better performance.

The FWHM for each axis is plotted for each plane in Fig. 4. The values for the x axis are plotted for each transverse slice, while the y and z axis are plotted for the sagital planes. In the x and z directions, a notable improvement of 2-3 mm in FWHM is observed for the span 1 reconstruction. In the y axis there was no noticeable difference.

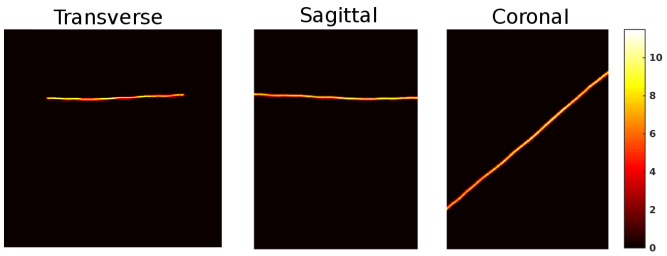

Fig. 3. Maximum intensity projections of the reconstructed image of the line source acquisition in the transverse, sagittal and coronal planes.

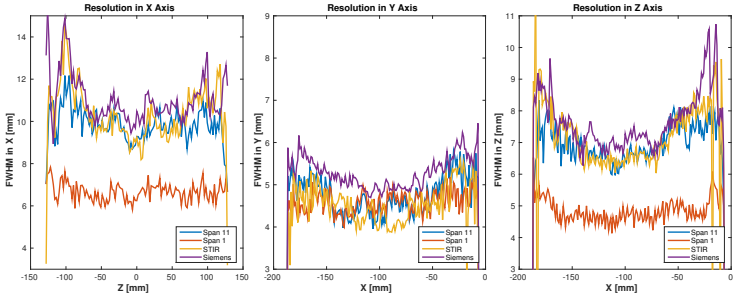

Fig. 4. FWHM in the x (left), y (center) and z (right) axes for different span 11 versions.

IV. Conclusions

A reconstruction algorithm without axial compression was implemented for the Biograph mMR and its general properties were verified using a NEMA IQ phantom acquisition and using STIR as a reference. In addition, we proposed a method to evaluate the SNR in the reconstructed images of the phantom when scatter correction was not applied. Using a line source, we showed that a meaningful improvement in resolution in the x and z axes is achieved when there is not axial compression. The reason why in the y axis there was not any improvement is because the line was placed in an almost fixed y coordinate and, then, there is no blurring effect in the y direction when averaging over adjacent oblique sinograms.

References

[1] B. Bendriem and D. W. Townsend, The Theory and Practice of 3D PET. Springer, 1998.

[2] G. Delso, S. Frst et al, "Performance Measurements of the Siemens mMR Integrated Whole-Body PET/MR Scanner," Journal of Nuclear Medicine, vol. 52, pp. 1914-1922, December 01, 2011.

[3] H. M. Hudson and R. S. Larkin et al, "Accelerated Image Reconstruction Using Ordered Subsets of Projection Data," IEEE Trans. Med. Img., Vol. 13, No. 4, December 1994.

[4] R. L. Siddon, "Fast calculation of the exact radiological path for a three-dimensional CT," J. Med. Phys., Vol. 12, No. 2, 1985.

[5] NVIDIA Corporation, "CUDA Programming Guide 7.5", September 2015.

[6] R. D. Badawi and P. K. Marsden, "Developments in component-based normalization for 3D PET," Phys. Med. Biol., vol. 44, pp. 571-594, 1999.

[7] K. Thielemans, C. Tsoumpas et al, STIR: Software for Tomographic Image Reconstruction Release 2," Physics in Medicine and Biology, 57 (4), 2012 pp.867-883.

[8] P. Markiewicz, K. Thielemans et al, "Image reconstruction of mMR PET data using the open source software STIR," EJNMMI Physics, vol. 1, 2014.

[9] National Electrical Manufacters Association, "NEMA NU2-2001: Performance Measurements of Positron Emission Tomographs," Rosslyn VA, 2001.